

Detection of the Spatiotemporal Trends of Mercury in Lake Erie Fish Communities: A Bayesian Approach

M. Ekram Azim,[†] Ananthavalli Kumarappah,[†] Satyendra P. Bhavsar,^{‡,§} Sean M. Backus,^{||} and George Arhonditsis^{*,†,§}

[†]Ecological Modeling Laboratory, Department of Physical and Environmental Sciences, University of Toronto, Toronto, Ontario M1C 1A4, Canada

[‡]Environmental Monitoring and Reporting Branch, Ontario Ministry of the Environment, Toronto, Ontario M9P 3V6, Canada

[§]Centre for Environment, University of Toronto, Toronto, Ontario M5S 3E8, Canada

^{||}Water Quality Monitoring & Surveillance Division, Water Science and Technology Directorate, Environment Canada, Burlington, Ontario L7R 4A6, Canada

 Supporting Information

ABSTRACT: The temporal trends of total mercury (*THg*) in four fish species in Lake Erie were evaluated based on 35 years of fish contaminant data. Our Bayesian statistical approach consists of three steps aiming to address different questions. First, we used the exponential and mixed-order decay models to assess the declining rates in four intensively sampled fish species, i.e., walleye (*Stizostedion vitreum*), yellow perch (*Perca flavescens*), smallmouth bass (*Micropterus dolomieu*), and white bass (*Morone chrysops*). Because the two models postulate monotonic decrease of the *THg* levels, we included first- and second-order random walk terms in our statistical formulations to accommodate nonmonotonic patterns in the data time series. Our analysis identified a recent increase in the *THg* concentrations, particularly after the mid-1990s. In the second step, we used double exponential models to quantify the relative magnitude of the *THg* trends depending on the type of data used (skinless-boneless fillet versus whole fish data) and the fish species examined. The observed *THg* concentrations were significantly higher in skinless boneless fillet than in whole fish portions, while the whole fish portions of walleye exhibited faster decline rates and slower rates of increase relative to the skinless boneless fillet data. Our analysis also shows lower decline rates and higher rates of increase in walleye relative to the other three fish species examined. The food web structural shifts induced by the invasive species (dreissenid mussels and round goby) may be associated with the recent *THg* trends in Lake Erie fish.

INTRODUCTION

The elevated concentrations of toxic, persistent, and bioaccumulative contaminants were first detected in the Great Lakes sediments and fish in the late 1960s/early 1970s.¹ Subsequently, the toxic effects of these chemicals were reported in wildlife² and humans.³ In response to increased public pressure and advocacy for virtual elimination of persistent toxic pollutants from the Great Lakes, various regulatory actions were undertaken at different government levels, such as the Great Lakes Water Quality Agreement (*GLWQA*) in 1972 and its subsequent revision in 1978. The agreement also included a call for monitoring and research programs to identify the spatiotemporal trends of these toxic substances in sediments and biota.⁴ Implementation of these regulatory actions resulted in decreased levels of most contaminants in the Great Lakes environment through the 1980s. However, from the mid-1990s, the decline rates have been reported to be slower, stagnant, or even to have switched to increasing rates in recent years.^{5–7} The reasons for these unexpected trends are not fully known but existing hypotheses suggest a direct causal association with the food web alterations induced from invasive species in the Great Lakes^{8,9} and also indirect links with global warming.¹⁰ The reported contaminant trends could have also been influenced by many factors such as

the type of statistical analysis performed, data pooling across the locations, type of samples (whole fish versus fillet portions), seasonality, and lack of explicit consideration of important covariates such as the fish size, feeding habits, behavioral patterns, reproductive status, growth, and lipid content. Inappropriate data analysis and interpretation of statistical trends derived from incomplete information can conceivably provide misleading results. Therefore, a holistic approach that explicitly accounts for all the potential causal factors is essential to discern the actual fish contaminant trends and to elucidate the underlying ecological mechanisms.

Among the persistent, bioaccumulative, and toxic contaminants, mercury (*Hg*) is a particular concern in aquatic environments because of its microbial transformation into methylmercury (*MeHg*) in water and sediments¹¹ and its subsequent transfer to the higher trophic levels. This organic form of *Hg* can biomagnify by approximately 10⁶ times in top predators, thereby resulting in significantly higher total mercury (*THg*) concentrations

Received: September 8, 2010

Accepted: January 20, 2011

Revised: January 14, 2011

Published: February 17, 2011

Table 1. Basic Statistics of Mercury Concentrations ($\mu\text{g/g}$ Wet Weight) in Whole Fish (WF) Samples for Walleye and Skinless-Boneless Fillet (SBF) Samples for Walleye and Three Other Fish Species in Lake Erie

| species | N | mean | SD | median | lower quart. | upper quart. | skewness | kurtosis |
|---|------|-------|-------|--------|--------------|--------------|----------|----------|
| Walleye (WF) <i>Stizostedion vitreum</i> | 757 | 0.122 | 0.072 | 0.107 | 0.080 | 0.150 | 2.526 | 10.538 |
| Walleye (SBF) <i>Stizostedion vitreum</i> | 1839 | 0.199 | 0.132 | 0.160 | 0.110 | 0.250 | 2.549 | 10.914 |
| Yellow Perch <i>Perca flavescens</i> | 1242 | 0.102 | 0.103 | 0.070 | 0.050 | 0.110 | 4.420 | 28.304 |
| Smallmouth Bass <i>Micropterus dolomieu</i> | 714 | 0.173 | 0.123 | 0.140 | 0.090 | 0.210 | 2.375 | 7.824 |
| White Bass <i>Morone chrysops</i> | 1651 | 0.146 | 0.103 | 0.120 | 0.080 | 0.180 | 3.146 | 18.84 |

relative to the source water, even in areas remote from industrial sources.¹² Generally, existing evidence suggests the rate of mercury bioaccumulation in individual fish depends on its trophic level in the food chain, dietary patterns, age, and size. The scattered and contradictory information on the temporal trends of contaminants in the Great Lakes fish sparked a hot debate.¹³ Namely, while the health benefits of eating fish are widely advocated, there was a growing concern that individuals who eat considerable amounts of fish from the Great Lakes have greater exposure to toxic chemicals and therefore are subject to health risks.¹³ Fish consumption can be a major exposure route of MeHg in food for many human populations.^{14,15} Elevated exposure to mercury can affect the nervous system, kidney, liver, and reproductive organs of human body. Some notable indices for neurotoxicity in humans include neuronal loss, ataxia, visual disturbances, impaired hearing, and death.¹⁴ In this regard, based on the mercury concentrations in fish reported from the ongoing Sport Fish Contaminant Monitoring Program (SFCMP), fish consumption advisories are published in Province of Ontario (Canada) with recommendations for limited fish consumption, ranging from zero to 8 meals per month depending on the vulnerability of the human population.¹⁶

In this study, a systematic and rigorous trend analysis was undertaken based on a 35-year fish mercury data set for Lake Erie. Our statistical analysis consisted of several models founded upon Bayesian formulations that aim to address different questions. First, we used the exponential and mixed-order decay models to assess the declining rates in four intensively studied fish species, i.e., walleye (*Stizostedion vitreum*), yellow perch (*Perca flavescens*), smallmouth bass (*Micropterus dolomieu*), and white bass (*Morone chrysops*). Because the two models postulate monotonic decrease of the Hg levels, we included random-walk error terms to accommodate nonmonotonic patterns in the time series data. In the second step, we used double exponential models to quantify the relative magnitude of the Hg trends depending on the type of data used (skinless-boneless fillet versus whole fish data) and the fish species examined. Finally, using skinless boneless fillet data, we introduced a hierarchical configuration of the double exponential model to examine to what extent the Hg temporal trends differ among different locations in Lake Erie.

METHODS

Data Set Description. The present study is based on the provincial (Ontario Ministry of the Environment; OMOE, Canada) skin-off dorsal fillet measurements used for fish consumption advisories, and the federal (Environment Canada; EC) whole fish measurements used to assess overall environmental contamination and risk to fish and fish-consuming wildlife. The fish species considered in our analysis were selected on the basis of data availability and commercial importance. We examined

four intensively sampled species viz., walleye (*Stizostedion vitreum*), yellow perch (*Perca flavescens*), smallmouth bass (*Micropterus dolomieu*), and white bass (*Morone chrysops*), while the number of observations in each species is given in Table 1. The detection of the mercury trends was based on whole fish (WF) and skinless-boneless fillet (SBF) samples for walleye and only SBF samples for the remaining fish species. The whole-fish samples were collected from Pelee Island in the western part of Lake Erie, while the fillet samples were collected from four different regions on the Canadian side of Lake Erie viz., 1: Western Basin, 2: Central Basin, 3: Long Point Bay, and 4: Eastern Basin (Figure 1 in the Supporting Information or Figure 1-ESM). The Eastern Basin of the Lake Erie is relatively deep with an average depth of 25 m and is characterized by relatively limited interactions between the water column and the sediments.¹⁷ By contrast, the Western Basin of Lake Erie is shallow, with a mean depth of 7.3 m and therefore allows significant contaminant transfer from the sediment to the water column; especially during episodic sediment resuspension events. The latter basin also receives a significant amount of chemical contaminants from the Detroit River.¹⁷

Mercury Analysis. Total mercury analysis for the OMOE samples was conducted at the OMOE laboratory in Toronto according to the OMOE method HGBIO-E3057. The EC samples were analyzed at the National Laboratory for Environmental Testing (NLET) using NLET method 2801. Both methods are briefly described in the Supporting Information.

Modeling Framework. Our approach comprises three steps that aim to detect the presence of statistically significant non-monotonic trends associated with the fish Hg concentrations (*step I*), to quantify the relative magnitude of these decreasing and/or increasing trends among the different fish species examined (*step II*), and to assess if the temporal trends vary among the different locations in Lake Erie (*step III*). Bayesian inference was used as a means for estimating model parameters due to its ability to include prior information in the modeling exercise and to explicitly handle the model structure and parameter uncertainty.¹⁸ Bayesian inference treats each parameter θ as random variable and uses the likelihood function to express the relative plausibility of obtaining different values of this parameter when particular data have been observed

$$\pi(\theta|data) = \frac{\pi(\theta)L(data|\theta)}{\int_{\theta} \pi(\theta)L(data|\theta)d\theta} \quad (1)$$

where $\pi(\theta)$ represents our prior statements regarding the probability distribution that more objectively depicts the existing knowledge on the θ values, $L(data|\theta)$ corresponds to the likelihood of observing the data given the different θ values, and $\pi(\theta|data)$ is the posterior probability that expresses our updated beliefs on the θ values after the existing data from the system are

considered. The denominator in eq 1 is the expected value of the likelihood function and acts as a scaling constant that normalizes the integral of the area under the posterior probability distribution.

Step I-Exponential Decay Models with Random Walk Terms. The first step of the analysis was based on the exponential decay and mixed-order models⁵

$$Hg_t = Hg_0 e^{kt} + \delta_t + \varepsilon \tag{2}$$

$$Hg_t = \{Hg_0^{1-\varphi} - kt(1-\varphi)\}^{(1/\varphi)} + \delta_t + \varepsilon \tag{3}$$

where Hg_t is the mercury concentration in year t ; Hg_0 is the mercury concentration at $t = 0$; k is the decay coefficient; and φ is the order of the reaction. A fundamental weakness of the two models is the postulation of a monotonic decrease of the Hg levels and therefore their inability to capture systematic deviations from this trend. To accommodate possible nonmonotonic patterns in the time series data, we included (zero mean) random error terms δ_t representing the annual deviations from the trajectory delineated by the two equations. To reflect the prior belief that these annual discrepancies are correlated, we assumed a first-order random walk prior specified as^{19,20}

$$p(\delta_t | \delta_{-t}, \omega^2) \sim \begin{cases} N(\delta_{t+1}, \omega^2) \text{ for } t = 1 \\ N\left(\frac{\delta_{t-1} + \delta_{t+1}}{2}, \frac{\omega^2}{2}\right) \text{ for } t = 2, \dots, T-1 \\ N(\delta_{t-1}, \omega^2) \text{ for } t = T \end{cases} \tag{4}$$

where δ_{-t} denotes all elements of δ_t except from the error associated with a particular year t , ω^2 is the conditional variance, and the prior densities $p(\omega^2)$ were based on conjugate inverse-gamma (0.001, 0.001) distributions. This statistical approach implies that the first-order differences of the annual Hg levels are smooth and that the probability of sudden jumps between consecutive years is unlikely. Alternatively, we examined a second-order random walk prior for δ_t representing prior beliefs that the rate of change (gradient) of the contaminant concentrations over the study period was smooth

$$p(\delta_t | \delta_{-t}, \omega^2) \sim \begin{cases} N(2\delta_{t+1} - \delta_{t+2}, \omega^2) \text{ for } t = 1 \\ N\left(\frac{2\delta_{t-1} + 4\delta_{t+1} - \delta_{t+2}}{5}, \frac{\omega^2}{5}\right) \text{ for } t = 2 \\ N\left(\frac{-\delta_{t-2} + 4\delta_{t-1} + 4\delta_{t+1} - \delta_{t+2}}{6}, \frac{\omega^2}{6}\right) \text{ for } t = 3, \dots, T-2 \\ N\left(\frac{-\delta_{t-2} + 4\delta_{t-1} + 2\delta_{t+1}}{5}, \frac{\omega^2}{5}\right) \text{ for } t = T-1 \\ N(-\delta_{t-2} + 2\delta_{t-1}, \omega^2) \text{ for } t = T \end{cases} \tag{5}$$

Finally, the ε term represents the measurement error and follows a Gaussian distribution, $N(0, \sigma_\varepsilon^2)$, where the prior density $p(\sigma_\varepsilon^2)$ was again based on conjugate inverse-gamma (0.001, 0.001) distribution.

Step II-Double Exponential Decay Models. The second phase of our analysis uses double exponential decay models to

quantify the relative magnitude of the Hg trends depending on the fish species examined and the type of data used (skinless-boneless fillet versus whole fish data)

$$Hg_t = Hg_{01} e^{k_1 t} + Hg_{02} e^{k_2 t} + \varepsilon \tag{6}$$

This model typically suggests that the temporal variability of the Hg concentrations is driven by two different factors/sources with distinct initial mercury concentrations, Hg_{01} and Hg_{02} , and rates of change, k_1 and k_2 . In our analysis, k_1 and k_2 were designed to correspondingly assess the magnitude of potential decreasing and increasing trends during the study period. Implicit in this statistical configuration is the idea that there are two effective Hg sources supplying the individual fish species, one of which declines and the other is increasing through time. In this case, the ε term represents the typical model error and follows a Gaussian distribution, $N(0, \sigma^2)$, with a prior density $p(\sigma^2)$ based on the conjugate inverse-gamma (0.001, 0.001) distribution.

Step III-Bayesian Hierarchical Models. The next phase of our analysis examines to what extent the Hg temporal trends differ among different locations in Lake Erie using the walleye skinless boneless fillet data. To account for site-specific differences, a hierarchical model was developed to predict the posterior probabilities of the site-specific k_1 and k_2 coefficients. The hierarchical formulation used in this analysis is summarized as follows²¹

$$\begin{aligned} \log(y_{ijt}) &\sim N(f(\theta_j, t), \tau^2) \\ \theta_j &\sim N(\theta, \sigma_j^2) \\ \theta &\sim N(\mu, \sigma^2) \\ \mu &\sim N(0, 10000) \end{aligned} \tag{7}$$

$$1/\tau^2, 1/\sigma^2 \sim \text{gamma}(0.001, 0.001)$$

where y_{ijt} denotes the i THg value observed in the site j and year t ; $f(\theta_j, t)$ is the double exponential model; τ^2 is the model error variance; θ_j represents the site-specific parameter sets; θ corresponds to the global parameters; μ and σ^2 are the mean and variance of the hyperparameters, respectively; and σ_j^2 is the group-specific variance; $N(0, 10000)$ is the normal distribution with mean 0 and variance 10000, and $\text{gamma}(0.001, 0.001)$ is the gamma distribution with shape and scale parameters of 0.001. The prior distributions for $1/\tau^2$, $1/\sigma^2$, and μ are considered “noninformative” or vague. We also examined the impact of the latter prior vis-à-vis the following three alternative distributions: (i) a gamma prior with shape and scale parameters of 0.1; (ii) a uniform prior distribution on the standard deviation scale in the range (0,100); and (iii) a half normal distribution truncated at zero and placed on the standard deviation scale. We found that the results presented herein are pretty robust to the selection of this prior and the inference drawn practically remained unaltered.

Sensitivity Analysis. The Bayesian configuration of the single exponential models and the mixed-order models was based on informative Hg_0 priors following normal distributions with the mean and standard deviation values derived from the first year when observed values for each fish species exist (called *Prior 1* herein). To determine the robustness of the reported results, the first-order exponential decay model was run using four different Hg_0 priors. Specifically, we used noninformative uniform/flat parameter distributions (*Prior 2*), normal (*Prior 3*) and log-normal (*Prior 4*) Hg_0 distributions parametrized such that 99% of the respective values were lying within the minimum and maximum mercury concentrations in the first year examined,

Table 2. Posterior Estimates (Mean Values \pm Standard Deviations) for the Models Used To Describe the Temporal Trends of Mercury Concentrations in Walleye (WF and SBF Portions), Yellow Perch (SBF), Smallmouth Bass (SBF), and White Bass (SBF)

| models | parameters | walleye WF | walleye SBF | yellow perch | smallmouth bass | white bass |
|--|------------|--------------------|--------------------|--------------------|--------------------|--------------------|
| exponential model with 1 st order smoothing | DIC | 1057 | 2516 | 2084 | 1084 | 2516 |
| | Hg_0 | 0.151 \pm 0.061 | 0.375 \pm 0.136 | 0.468 \pm 0.284 | 0.293 \pm 0.157 | 0.141 \pm 0.058 |
| | k | -0.017 \pm 0.025 | -0.049 \pm 0.025 | -0.084 \pm 0.038 | -0.037 \pm 0.038 | -0.002 \pm 0.031 |
| | ω | 0.146 \pm 0.037 | 0.252 \pm 0.041 | 0.365 \pm 0.071 | 0.323 \pm 0.062 | 0.396 \pm 0.058 |
| | σ_e | 0.487 \pm 0.013 | 0.481 \pm 0.008 | 0.590 \pm 0.012 | 0.528 \pm 0.014 | 0.523 \pm 0.009 |
| exponential model with 2 nd order smoothing | DIC | 1020 | 2486 | 2188 | 1026 | 2436 |
| | Hg_0 | 0.222 \pm 0.099 | 0.389 \pm 0.171 | 0.509 \pm 0.225 | 0.303 \pm 0.181 | 0.136 \pm 0.065 |
| | k | -0.039 \pm 0.042 | -0.050 \pm 0.028 | -0.095 \pm 0.030 | -0.033 \pm 0.051 | 0.004 \pm 0.041 |
| | ω | 0.051 \pm 0.025 | 0.345 \pm 0.067 | 0.408 \pm 0.099 | 0.296 \pm 0.075 | 0.604 \pm 0.094 |
| | σ_e | 0.492 \pm 0.013 | 0.481 \pm 0.008 | 0.591 \pm 0.012 | 0.537 \pm 0.015 | 0.523 \pm 0.009 |
| mixed model with 1 st order smoothing | DIC | 940 | 1662 | 1839 | 880 | 2102 |
| | Hg_0 | 0.142 \pm 0.054 | 0.275 \pm 0.129 | 0.376 \pm 0.226 | 0.223 \pm 0.106 | 0.171 \pm 0.084 |
| | k | 0.240 \pm 0.285 | 0.276 \pm 0.276 | 0.514 \pm 0.283 | 0.242 \pm 0.268 | 0.203 \pm 0.256 |
| | φ | 2.450 \pm 0.508 | 2.44 \pm 0.52 | 1.95 \pm 0.38 | 2.423 \pm 0.520 | 2.452 \pm 0.529 |
| | ω | 0.136 \pm 0.034 | 0.243 \pm 0.040 | 0.341 \pm 0.069 | 0.316 \pm 0.062 | 0.397 \pm 0.058 |
| | σ_e | 0.487 \pm 0.013 | 0.481 \pm 0.008 | 0.590 \pm 0.012 | 0.528 \pm 0.014 | 0.523 \pm 0.009 |
| mixed model with 2 nd order smoothing | DIC | 735 | 1481 | 1073 | 850 | 2508 |
| | Hg_0 | 0.171 \pm 0.085 | 0.297 \pm 0.148 | 0.315 \pm 0.219 | 0.228 \pm 0.120 | 0.141 \pm 0.028 |
| | k | 0.300 \pm 0.301 | 0.281 \pm 0.275 | 0.423 \pm 0.290 | 0.237 \pm 0.270 | 0.143 \pm 0.211 |
| | φ | 2.385 \pm 0.491 | 2.39 \pm 0.52 | 1.98 \pm 0.46 | 2.440 \pm 0.514 | 2.533 \pm 0.535 |
| | ω | 0.048 \pm 0.024 | 0.346 \pm 0.067 | 0.405 \pm 0.100 | 0.360 \pm 0.092 | 0.604 \pm 0.093 |
| | σ_e | 0.492 \pm 0.013 | 0.481 \pm 0.008 | 0.591 \pm 0.012 | 0.531 \pm 0.0145 | 0.523 \pm 0.009 |
| double exponential model | DIC | 1120 | 2754 | 2381 | 1265 | 3027 |
| | Hg_{01} | 0.099 \pm 0.018 | 0.230 \pm 0.010 | 0.173 \pm 0.015 | 0.164 \pm 0.021 | 0.041 \pm 0.015 |
| | Hg_{02} | 0.071 \pm 0.013 | 0.041 \pm 0.009 | 0.034 \pm 0.006 | 0.071 \pm 0.012 | 0.110 \pm 0.008 |
| | k_1 | -0.422 \pm 0.202 | -0.133 \pm 0.018 | -0.195 \pm 0.027 | -0.216 \pm 0.050 | -0.442 \pm 0.148 |
| | k_2 | 0.022 \pm 0.008 | 0.056 \pm 0.008 | 0.026 \pm 0.006 | 0.032 \pm 0.007 | 0.005 \pm 0.003 |
| | σ | 0.062 \pm 0.006 | 0.067 \pm 0.004 | 0.152 \pm 0.012 | 0.110 \pm 0.012 | 0.123 \pm 0.009 |

and a multivariate normal prior that accounts for the covariance between the parameters Hg_0 and k (Prior 5).

Model Computations. Sequence of realizations from the model posterior distributions were obtained using Markov chain Monte Carlo (MCMC) simulations. Specifically, we used the general normal-proposal Metropolis algorithm as implemented in the WinBUGS software;²² this algorithm is based on a symmetric normal proposal distribution, whose standard deviation is adjusted over the first 4000 iterations such as the acceptance rate ranges between 20% and 40%. We used three chain runs of 80,000 iterations, and samples were taken after the MCMC simulation converged to the true posterior distribution. Convergence was assessed using the modified Gelman-Rubin convergence statistic. Generally, we noticed that the sequences converged very rapidly (\approx 1000 iterations), and the summary statistics reported in this study were based on the last 75,000 draws by keeping every 20th iteration (thin=20) to avoid serial correlation. The accuracy of the posterior parameter values was inspected by assuring that the Monte Carlo error for all parameters was less than 5% of the sample standard deviation. The models presented in this analysis were compared using the deviance information criterion (DIC), a Bayesian measure of model fit and complexity.²³

RESULTS

The summary statistics of the total mercury (THg) concentrations in the fish species examined are shown in Table 1. For

walleye, the THg concentrations were more than 60% higher in skinless boneless fillet relative to whole fish portions, although we caution that these concentrations were not derived from concurrent samples and therefore may partly reflect the different philosophies (and associated sampling practices) of the two data sets used. Further, higher concentrations were recorded in walleye (mean 0.199 and median 0.160 $\mu\text{g/g}$ wet weight), followed by smallmouth bass (0.173 and 0.140 $\mu\text{g/g}$ wet weight) and white bass (0.146 and 0.120 $\mu\text{g/g}$ wet weight), while yellow perch (0.102 and 0.070 $\mu\text{g/g}$ wet weight) was characterized by relatively lower concentrations. The high standard deviation and interquartile range values reflect the substantial inter- and intra-annual variability associated with the mercury levels of the individual fish species. The high positive values of skewness and kurtosis are indicative of right skewed and leptokurtic distributions, and therefore the logarithmic transformation was implemented for the subsequent analysis.

The posterior estimates for the models used to describe the temporal mercury trends in walleye WF and SBF portions are shown in Table 2. The exponential decay model, expressing continuously decreasing trends in THg concentrations at an ever-slowing rate toward a zero concentration, suggests higher decay rates in the walleye SBF ($k = -0.049 \pm 0.025 \text{ yr}^{-1}$ and $k = -0.050 \pm 0.028 \text{ yr}^{-1}$) relative to the WF ($k = -0.017 \pm 0.025 \text{ yr}^{-1}$ and $k = -0.039 \pm 0.042 \text{ yr}^{-1}$) data. The higher values of the coefficient of variation (standard deviation/mean value) associated with

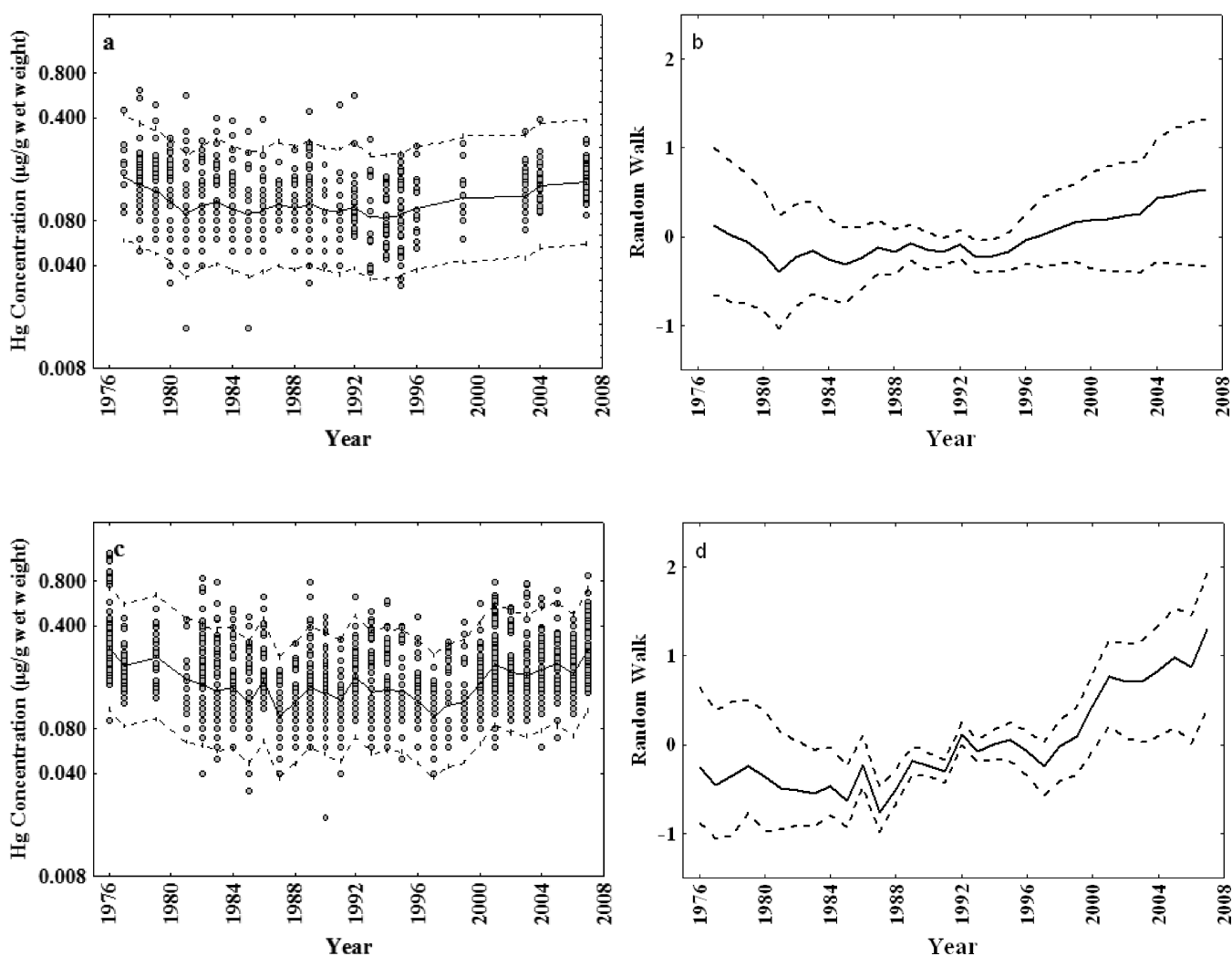


Figure 1. Walleye mercury concentrations over time (1976–2007) using the exponential decay model with (a, b) whole fish, and (c, d) skinless-boneless fillet data for Lake Erie. The circles indicate the observed values, while the solid and dashed lines correspond to the median and the 95% credible intervals of the posterior predictive distributions, respectively. The δ_t annual values correspond to the first-order random walk terms introduced to account for the structural deficiencies of the single exponential model.

the *WF* data indicate that the latter estimates are not well determined. We also note that the lower *DIC* values render support to the second-order temporal smoothing relative to the first order approach with both *WF* and *SBF* walleye data. The predicted *THg* concentrations in the *WF* portions decreased until the early 1980s and then remained more or less constant through 1994, after which continually increased at a relatively slow rate until the recent years (Figure 1a). The δ_t (random walk) terms were used to detect the systematic errors resulting from the structural inadequacies of the single exponential model. In particular, the positive values of the structural error terms during the second half of the survey period represent the inadequacy of the exponential decay model to capture the concurrent increasing trends (Figure 1b). Notably, the rate of increase in the *WF* portions was slower in recent years as compared to the rate in *SBF* portions (Figure 1d). In particular, the *THg* concentrations in *SBF* portions declined gradually from the 1970s until 1986, thereafter they began to increase at a slower rate through 1992. Then, a sharp decline was noticed until 1997, after which the concentrations increased rapidly until the last sampling year 2007 (Figure 1c). Importantly, our sensitivity ana-

lysis of the exponential decay model showed that the conclusions drawn upon the general *THg* temporal patterns are robust, although that actual parameter estimates can differ depending on the prior assumptions made about the relative plausibility of their values (Table 1-ESM and Figure 2-ESM).

The parameter estimates of the exponential decay models for the other three fish species are also presented in Table 2, while the corresponding predictions and δ_t terms can be found in the Supporting Information (Figure 3-ESM). Similar to the walleye patterns, smallmouth bass and yellow perch show increasing (but weaker) trends approximately after the mid-1990s, whereas the structural error terms of the white bass model revolved around the zero value throughout the study period. The model with the first order temporal smoothing correction resulted in higher initial *THg* concentrations and decay rates for yellow perch ($Hg_0 = 0.468 \pm 0.284 \mu\text{g THg/g}$, $k = -0.084 \pm 0.038 \text{ yr}^{-1}$) followed by smallmouth bass ($Hg_0 = 0.293 \pm 0.157 \mu\text{g THg/g}$, $k = -0.037 \pm 0.038 \text{ yr}^{-1}$) and white bass ($Hg_0 = 0.141 \pm 0.058 \mu\text{g THg/g}$, $k = -0.002 \pm 0.031 \text{ yr}^{-1}$). With the second-order temporal smoothing, the *DICs* decreased from 1084 to 1026 for smallmouth bass and from 2516 to 2436 for white bass but increased from 2084 to 2188 for yellow perch. Thus,

although the results are not always consistent, the present analysis indicates that the second-order smoothing is more favorably supported when we consider both model performance and complexity. It is also interesting to note that the predicted initial *THg* concentrations and decay coefficients were fairly similar between the two statistical configurations examined.

The mixed order model, accommodating declines toward zero but at rates that slow more rapidly than rates in an exponential model would, had lower *DIC* values relative to both single and double exponential decay models (Table 2). The decay rates were slightly higher in *SBF* than in *WF* walleye data for the first order, and the opposite was true for the second-order temporal smoothing formulations. However, both statistical configurations predicted significantly higher initial *Hg* concentrations in *SBF* than in *WF* portion data. We also found relatively similar estimates of the reaction order (φ) between the two types of data. The trends of the *THg* concentrations in both walleye *WF* and *SBF* portions throughout the study period were fairly similar to the exponential decay model (Figure 4a,c in the SI), although the credible intervals for the structural error terms δ were somewhat narrower (Figure 4b,d in the SI). The relative values of the *k* posterior estimates were similar to those derived from the exponential decay models, i.e., yellow perch > walleye > smallmouth bass > white bass (see also Figure 5-ESM). However, the predicted decay coefficients were accompanied by substantial standard deviations (coefficients of variation ≈ 70 –114%), which may counterbalance the support provided by the lower *DIC* values.

After establishing the presence of nonmonotonic temporal patterns in the mercury concentrations, the rationale behind the use of the double exponential model was to explicitly quantify the rates of decrease (k_1) and increase (k_2). We primarily highlight that the absolute values of the decay coefficients (k_1) were at least twice as high relative to the *k* values derived from the single exponential models (Table 2). This finding suggests that the predictions of the latter equation coupled with a random walk term can only be compared qualitatively with those derived from the double exponential model. Notably, the same model results in fairly well determined parameter estimates relative to those reported in the first phase of our analysis. According to the double exponential model, the walleye *WF* portions exhibited three times higher decrease in mercury concentrations ($k_1 = -0.422 \pm 0.202 \text{ yr}^{-1}$) than the *SBF* data ($k_1 = -0.133 \pm 0.018 \text{ yr}^{-1}$). By contrast, the *WF* portions had 2.5 times lower rate of increase ($k_2 = 0.022 \pm 0.008 \text{ yr}^{-1}$) as compared to the ones derived from the *SBF* data ($k_2 = 0.056 \pm 0.008 \text{ yr}^{-1}$). The shift from decreasing to increasing trends became evident in 1986 for the *WF* (Figure 6a in the SI) and in 1990 for the *SBF* data (Figure 6b in the SI). Unlike the single exponential decay model, the highest decay rates were recorded in white bass ($k_1 = -0.442 \pm 0.148 \text{ yr}^{-1}$) followed by smallmouth bass ($k_1 = -0.216 \pm 0.050 \text{ yr}^{-1}$), yellow perch ($k_1 = -0.195 \pm 0.027 \text{ yr}^{-1}$) and walleye ($k_1 = -0.133 \pm 0.018 \text{ yr}^{-1}$) (Table 2). Yet, the highest rates of increase in *THg* concentrations were recorded in walleye ($k_2 = 0.056 \pm 0.008 \text{ yr}^{-1}$) followed by smallmouth bass ($k_2 = 0.032 \pm 0.007 \text{ yr}^{-1}$), yellow perch ($k_2 = 0.026 \pm 0.006 \text{ yr}^{-1}$) and white bass ($k_2 = 0.005 \pm 0.003 \text{ yr}^{-1}$), respectively. Notably, the recent rates of increase were significantly lower than the decrease rates until the late 1980s for all four species examined (Figure 6-ESM).

DISCUSSION

Heavy metal accumulation in fish mainly involves the biological sequestering of substances that enter the body through

epidermal contact with the substance, respiration, and food intake. In particular, the dietary intake can contribute up to 90% of the methyl mercury (*MeHg*) concentrations in fish tissues.²⁴ The level at which a given substance is bioaccumulated depends on the rate of uptake, the path through which the substance is transferred (e.g., gills, skin contact, ingested with food), the elimination rate of the substance from the organism, transformation of the substance by metabolic processes, the lipid content of the organism, the hydrophobicity of the substance, and other environmental factors. Generally, bioaccumulation occurs at each step of the food chain, resulting in top predators amassing high concentrations of contaminants, while *THg* accumulation rate in top predators also increases with increasing age and size.²⁵ Among the four fish species examined in the present study, the top predators walleye and smallmouth bass had indeed the highest observed body *THg* concentrations, while the *THg* levels in walleye were higher in skinless boneless fillet than in whole fish portions.

Relating the latter pattern with the fact that *MeHg* is typically the predominant fraction (>90%) of *THg* in edible fish tissue samples,^{9,26} we can infer that *MeHg* should also constitute a substantial part of our recorded fish mercury levels which in turn may be associated with the two major predictions of our double exponential models regarding the temporal trends of mercury contamination in Lake Erie fish communities: (i) the walleye *THg* concentrations appear to have been subjected to rapid decrease rates during the earlier years and (more recently) to slower increase rates in whole fish portions than in fillet tissues; and (ii) top predators with relatively higher mercury concentrations were generally characterized by lower decline and/or higher increase rates. *MeHg* is an intracellular organo-metallic contaminant that has high affinity to the sulfite group of host proteins, and thus is efficiently transported into the muscle tissues and excreted slower than any other inorganic form of metals.²⁶ Existing evidence suggests that several important physical (e.g., lake area, epilimnetic temperature), chemical (e.g., organic matter, pH, *Hg* aging, iron levels, balance between sulfate and sulfide), and biological (e.g., type and activity of bacteria, food web structure, fish population age and growth rates) factors can potentially control *MeHg* bioaccumulation and dramatically affect the transfer of *Hg* load into *MeHg* in fish.^{26,27} In Lake Erie, there are several reasons (e.g., extent of the nearshore zone, anoxic conditions) to believe that *MeHg* accumulation occurs in the sediments and regularly contributes *MeHg* pulses to the overlying waters. Yet, Hogan et al.⁹ reported ratios of *MeHg* to *THg* equal to 0.2% for sediments, 30% for dreissenids, 65% for round gobies, and 93% for smallmouth bass. Thus, the fact that smallmouth bass *MeHg* concentrations are estimated to be 1000 times higher than in the Lake Erie sediments underscores, more than anything else, the *MeHg* capacity to immensely biomagnify and therefore to modulate the imprint of restoration actions on aquatic biota.

Consistent with Bhavsar et al.'s²⁸ recent findings, our analysis suggests that the declines in *THg* concentrations appears to have slowed down in almost all fish species (or even to have increased) after the invasion of dreissenids and round gobies in the late 1980s. These temporal patterns may be explained by Hogan et al.'s⁹ conceptual model which suggests that the invasion of exotic species has shifted the food web from a pelagic-based to a benthic-based one, thereby creating new trophodynamics for contaminant transfer to top predators. First, the introduction of zebra and quagga mussels has likely induced major changes in the

fluxes of heavy metals within the Lake Erie food web, because of their ability to bioaccumulate through profuse filtering of contaminated water and scavenging of phytoplankton and particulate matter.²⁹ While the precise quantification of the bioaccumulation of contaminants in aquatic animals is not a trivial exercise and is determined by the complex interplay among uptake efficiencies from food and water pathways (physiological assimilation and absorption efficiencies), filtration, ingestion, growth, and depuration rates of contaminants from the animals, dreissenid contaminant levels appear to covary with the corresponding sediment concentrations; especially in the shallow littoral areas of the western basin of Lake Erie where large sediment contaminant loads are experienced.²⁹ Dreissenids are good sentinels of the bioavailability of contaminants and can potentially elevate the likelihood of trophic transfer.³⁰ Further, their capacity to selectively remove particulate organic matter from the water column increases the dissolved-phase fraction of contaminants, which in turn can increase the body burdens of many aquatic organisms.⁸ Concomitant to the spread of dreissenid mussels, round goby invaded the Great Lakes and became extremely abundant in Lake Erie in 1996, causing major shift in diets and increased growth rates of top predators.³¹ As a benthic fish with diet mainly composed of dreissenids, round goby has the potential to accumulate contaminants and transfer them to the higher trophic levels through the food web.³² Consequently, the prospect of an increased reliance upon benthivorous round goby can possibly explain the increase *THg* rates of the top predators during the second half of our study period, despite the substantial decrease of the contemporaneous *THg* levels in the Lake Erie sediments.³³ The recent increase in *THg* concentrations in fish might also be linked to the global warming and other climatic variability. Elevated temperatures can increase *THg* concentrations in fish by increasing mercury methylation rates in sediments and *Hg* release from the watershed.²⁶ Global warming could also influence trophodynamics of the contaminants by altering lake phenologies and biotic community structures.³⁴

The Eastern Basin of Lake Erie is characterized by higher observed mean and median *THg* concentrations in walleye fish fillet (0.227 and 0.202 $\mu\text{g/g ww}$, respectively) as compared to the Western Basin (0.205 and 0.186 $\mu\text{g/g ww}$), despite the fact that the latter area receives substantial inputs from the Detroit River and other tributaries.¹⁷ Notably, the same basin was also characterized by greater rates of change (both decrease and increase) relative to the other three areas of the lake (Figure 7-ESM). The reasons for the somewhat counterintuitive trends are uncertain and might be related to the source and degree of *Hg* contamination, length and composition of food webs, tissue turnover rates of biota, biogeochemistry of the different locations, and home range of the fish species examined.³⁵ Although Western Basin is historically more polluted, its shallow depth, high productivity, and warm water might enhance the growth of walleye resulting in increased contaminant dilution.²⁶ Notably, the samples from the Eastern Basin were characterized from greater mean length (53.29 ± 10.04 cm) and weight (1704 ± 868 g) relative to those collected from the Western Basin (44.58 ± 8.44 cm and 973 ± 568 g). The latter finding may suggest a systematic bias introduced by the local sampling practices, which in turn invites the explicit consideration of all the possible covariates (e.g., length, gender, lipid content) that can potentially impede the detection of the actual temporal trends of fish contaminants and thus may misinform consumption advisories. Finally, another possible reason might be the lake-wide movement of walleye for

better food availability and/or environmental conditions. Therefore, this type of analysis may be more appropriate for localized/sedentary species (e.g., spottail shiners) and not for species with wider “home range” like walleye. To this end, we examined the observed *THg* levels in relatively localized yellow perch and found that the contaminant concentration was higher in fish collected from the Western Basin (0.136 $\mu\text{g THg/g ww}$) than in fish from the Eastern Basin (0.108 $\mu\text{g THg/g ww}$); that is, opposite to the walleye trends.

The addition of the temporally variant random error term δ in the statistical formulation examined has enabled the detection of nonmonotonic trends in our data set and therefore can conceivably overcome the structural inadequacies of models that have been traditionally used in the context of fish contaminant trend analysis.^{5,36,37} While admittedly the statistical formulation introduced is prone to data overfitting (e.g., the relatively similar values of the structural error covariance ω between the single exponential and mixed order models) and can weaken somewhat the signal/trend typically captured by the k coefficient (i.e., the random walk parameter estimates may sometimes be confounded with the exponential decay term), we believe that the proposed framework can be a useful exploratory tool to elucidate idiosyncratic cases typically encountered in fish contaminant data sets, such as the white bass temporal variability (Figure 3e in the Supporting Information). Namely, a careful inspection of the observed *THg* trends suggests a wax and wane pattern throughout the survey period which cannot be captured by any of the rigid model structure used so far (e.g., single or double exponential, mixed-order, nonzero asymptote). For example, the double exponential model resulted in a misleadingly high decay rate (-0.442 ± 0.148) and a nearly nonexistent increasing trend (0.005 ± 0.003), whereas the same pattern was quite faithfully depicted by the random error terms (Figures 3 and 5f in the Supporting Information). We also addressed one of the historical criticisms of the Bayesian approach regarding the use of subjective prior beliefs on the relative plausibility of different parameter values,³⁸ and our sensitivity analysis demonstrated that the inference drawn is quite robust on the different prior parameter specifications. Generally, our analysis identified as the most parsimonious approach the mixed order model combined with the second-order temporal smoothing, although we caution that the posterior estimates of the decay rates were almost consistently poorly determined.

Acknowledging the weaknesses of all the models used for detecting fish contaminant trends in time and space, one of the key messages that the present study aims to convey is the importance of adopting conceptually integrative modeling frameworks. For example, rather than picking the “best” of the five modeling configurations examined and then basing the delineation of the trajectories on that single “best-fit” model, we propose the Bayesian model averaging as a means for providing a weighted average description from all five approaches.⁵ In particular, the MCMC samples can be used to calculate the posterior probabilities for each model, which then provide the weights to combine the predictions from all models (Figure 2). The averaged predictions reinforce the U-shape pattern characterizing the walleye *SBF* (Figure 2a), and the weakly increasing trends recently followed by the walleye *WF* portions, the smallmouth bass and yellow perch *SBF* data (Figure 2b-d). Finally, it should also be noted that a follow-up dynamic linear modeling analysis (Sadraddini et al., submitted manuscript) has verified these temporal trends, even when we explicitly account for the fact

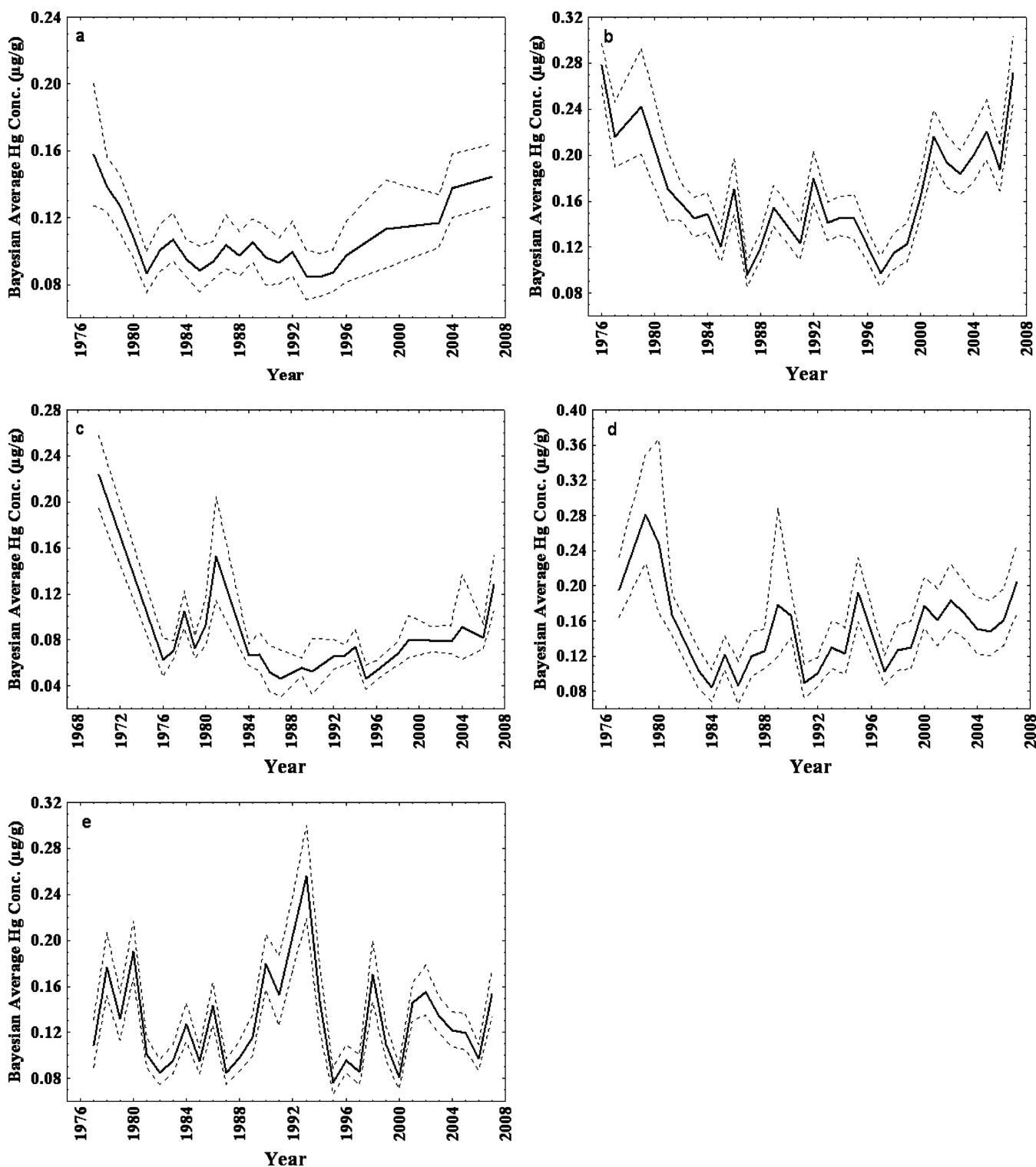


Figure 2. Mercury concentrations over time (1970–2007) using Bayesian Model Averaging (BMA) with (a) walleye whole fish, (b) walleye skinless-boneless fillet, (c) yellow perch skinless-boneless fillet, (d) smallmouth bass skinless-boneless fillet, and (e) white bass skinless-boneless fillet data for Lake Erie. The solid and dashed lines correspond to the mean concentrations and the 95% credible intervals, respectively.

that the fish length covaries with the THg concentrations and that different sized fish may have been sampled over time.

In conclusion, we used a Bayesian modeling framework that identified an increasing trend of THg concentrations in Lake Erie fish becoming particularly evident after the mid-90s. The observed THg concentrations were significantly higher in skinless

boneless fillet than in whole fish portions, while the whole fish data of walleye exhibited faster decline rates and slower rates of increase relative to the skinless boneless fillet samples. Our analysis also shows lower decline rate and higher rate of increase in walleye relative to smallmouth bass, yellow perch, and white bass, which underscores the importance of considering more

than one fish species for proper spatial/temporal trend assessments. Finally, we suggest that the recent increase in fish THg may be explained by structural shifts of the Lake Erie food web due to invasive species (dreissenid mussels and round goby). A logical next step would be the examination of a broader range of fish species along with the explicit consideration of all the possible factors (age, weight, sex, lipid content, class size) that can potentially obfuscate the detection of the real temporal THg trends.

■ ASSOCIATED CONTENT

S Supporting Information. Additional information related to sample extraction and mercury analysis and the sensitivity analysis of the exponential decay model along with the rest of the results of our modeling study. This material is available free of charge via the Internet at <http://pubs.acs.org>.

■ AUTHOR INFORMATION

Corresponding Author

*Phone: (416)208-4858. Fax: (416)287-7279. E-mail: georgea@utsc.utoronto.ca.

■ ACKNOWLEDGMENT

This project has received funding support from the Ontario Ministry of the Environment (Best in Science Research Program-Grant Funding Agreement 89002). Such support does not indicate endorsement by the Ministry of the contents of the study. All the material pertinent to this analysis is available upon request from the corresponding author.

■ REFERENCES

- (1) Fimreite, N.; Holsworth, W. N.; Keith, J. A.; Pearce, P. A.; Gruchy, I. M. Mercury in fish and fish-eating birds near sites of industrial contamination in Canada. *Can. Field-Nat.* **1971**, *85*, 211–220.
- (2) Gilbertson, M.; Morris, R. D.; Hunter, R. A. Abnormal chicks and PCB residue levels in eggs of colonial birds on the lower Great Lakes (1971–1973). *Auk* **1976**, *93*, 434–442.
- (3) Johnson, B. L.; Hicks, H. E.; Jones, D. E.; Cibulas, W.; Wargo, A.; De Rosa, C. T. Public health implications of persistent toxic substances in the Great Lakes and St. Lawrence basins. *J. Great Lakes Res.* **1998**, *24*, 698–722.
- (4) International Joint Commission (IJC). *A guide to the Great Lakes Water Quality Agreement: Background for the 2006 Governmental Review*; Canada and the United States, 2006; ISBN 1-894280-53-9.
- (5) Stow, C. A.; Lamon, E. C.; Qian, S. S.; Schrank, C. S. Will Lake Michigan lake trout meet the Great Lakes Strategy 2002 PCB reduction goal?. *Environ. Sci. Technol.* **2004**, *38*, 359–363.
- (6) Bhavsar, S. P.; Awad, E.; Fletcher, R.; Hayton, A.; Somers, K. M.; Kolic, T.; MacPherson, K.; Reiner, E. J. Temporal trends and spatial distribution of dioxins and furans in lake trout or lake whitefish from the Canadian Great Lakes. *Chemosphere* **2008**, *73*, S158–S165.
- (7) Gewurtz, S. B.; Bhavsar, S. P.; Jackson, D. A.; Fletcher, R.; Awad, E.; Moody, R.; Reiner, E. J. Temporal and spatial trends of organochlorines and mercury in fishes from the St. Clair River/Lake St. Clair corridor, Canada. *J. Great Lakes Res.* **2010**, *36*, 100–112.
- (8) Morrison, H. A.; Gobas, F.; Lazar, R.; Whittle, D. M.; Haffner, G. D. Projected changes to the trophodynamics of PCBs in the western Lake Erie ecosystem attributed to the presence of zebra mussels (*Dreissena polymorpha*). *Environ. Sci. Technol.* **1998**, *32*, 3862–3867.
- (9) Hogan, L. S.; Marschall, E.; Folt, C.; Stein, R. A. How non-native species in Lake Erie influence trophic transfer of mercury and lead to top predators. *J. Great Lakes Res.* **2007**, *33*, 46–61.
- (10) French, T. D.; Campbell, L. M.; Jackson, D. A.; Casselman, J. M.; Scheider, W. A.; Hayton, A. Long-term changes in legacy trace organic contaminants and mercury in Lake Ontario salmon in relation to source controls, trophodynamics, and climatic variability. *Limnol. Oceanogr.* **2006**, *51*, 2794–2807.
- (11) Sweet, L. I.; Zelikoff, J. T. Toxicology and Immunotoxicology of mercury: A comparative review in fish and humans. *J. Toxicol. Environ. Health B* **2001**, *4*, 161–205.
- (12) Fitzgerald, W. F.; Engstrom, D. R.; Mason, R. P.; Nater, E. A. The case for atmospheric mercury contamination in remote areas. *Environ. Sci. Technol.* **1998**, *32*, 1–7.
- (13) Johnson, B. L.; Hicks, H. E.; De Rosa, C. T. Key environmental human health issues in the Great Lakes and St. Lawrence River Basins. *Environ. Res.* **1999**, *80*, S2–S12.
- (14) FAO/WHO. *Joint FAO/WHO expert committee on food additives: summary and conclusions*. Sixty first meeting, Food and Agriculture Organization of the United Nations and World Health Organization, Rome, 2003.
- (15) Campbell, L. M.; Dixon, D. G.; Hecky, R. E. A review of mercury in Lake Victoria, East Africa: Implications for human and ecosystem health. *J. Toxicol. Environ. Health B* **2003**, *6*, 325–356.
- (16) Ontario Ministry of the Environment (MOE), *Guide to eating Ontario sport fish, 2009–2010*. Sport Fish Contaminant Monitoring Program, Environmental Monitoring and Reporting Branch, Etobicoke, Ontario, Canada.
- (17) Carter, D. S.; Hites, R. A. Fate and transport of Detroit River derived pollutants throughout Lake Erie. *Environ. Sci. Technol.* **1992**, *26*, 1333–1341.
- (18) Arhonditsis, G. B.; Qian, S. S.; Stow, C. A.; Lamon, E. C.; Reckhow, K. H. Eutrophication risk assessment using Bayesian calibration of process-based models: Application to a mesotrophic lake. *Ecol. Modell.* **2007**, *208*, 215–229.
- (19) Shaddick, G.; Wakefield, J. Modelling daily multivariate pollutant data at multiple sites. *J. R. Stat. Soc. Ser. C* **2002**, *51*, 351–372.
- (20) Arhonditsis, G. B.; Perhar, G.; Zhang, W.; Massos, E.; Shi, M.; Das, A. Addressing equifinality and uncertainty in eutrophication models. *Water Resour. Res.* **2008**, *44*, W01420, doi:10.1029/2007WR005862.
- (21) Wikle, C. K. Hierarchical Bayesian models for predicting the spread of ecological processes. *Ecology* **2003**, *84*, 1382–1394.
- (22) Lunn, D. J.; Thomas, A.; Best, N.; Spiegelhalter, D. WinBUGS—a Bayesian modelling framework: concepts, structure, and extensibility. *Stat. Comput.* **2000**, *10*, 325–337.
- (23) Spiegelhalter, D.; Best, N.; Carlin, B.; van der Linde, A. Bayesian measures of model complexity and fit. *J. Roy. Stat. Soc. B* **2002**, *64*, 583–639 & 699–700.
- (24) Wiener, J. G.; Krabbenhoft, D. P.; Heinz, G. H.; Scheuhammer, A. M. Ecotoxicology of mercury. In *Handbook of Ecotoxicology*, 2nd ed.; Hoffman, D. J., Rattner, B. A., Burton, G. A., Jr., Cairns, J., Jr., Eds.; CRC Press: Boca Raton, 2002.
- (25) Cabana, G.; Tremblay, A.; Kalff, J.; Rasmussen, J. B. Pelagic food chain structure in Ontario lakes: A determinant of mercury levels in lake trout (*Salvelinus namaycush*). *Can. J. Fish. Aquat. Sci.* **1994**, *51*, 381–389.
- (26) Munthe, J.; Bodaly, R. A.; Branfireun, B. A.; Driscoll, C. T.; Gilmour, C. C.; Harris, R.; Horvat, M.; Lucotte, M.; Malm, O. Recovery of mercury-contaminated fisheries. *Ambio* **2007**, *36*, 33–44.
- (27) Evans, M. S.; Lockhart, W. L.; Doetzel, L.; Low, G.; Muir, D.; Kidd, K.; Stephens, G.; Delaronde, J. Elevated mercury concentrations in fish in lakes in the Mackenzie River Basin: the role of physical, chemical and biological factors. *Sci. Total Environ.* **2005**, *351*–*352*, 479–500.
- (28) Bhavsar, S. P.; Gewurtz, S. B.; McGoldrick, D. J.; Keir, M. J.; Backus, S. M. Changes in mercury levels in Great Lakes fish between 1970s and 2007. *Environ. Sci. Technol.* **2010**, *44*, 3273–3279.
- (29) Kwan, K. H. M.; Chan, H. M.; De Lafontaine, Y. Metal contamination in zebra mussels (*Dreissena polymorpha*) along the St. Lawrence River. *Environ. Monit. Assess.* **2003**, *88*, 193–219.
- (30) Kwon, T. D.; Fisher, S. W.; Kim, G. W.; Hwang, H.; Kim, J. E. Trophic transfer and biotransformation of polychlorinated biphenyls in

zebra mussel, round goby, and smallmouth bass in Lake Erie, USA. *Environ. Toxicol. Chem.* **2006**, *25*, 1068–1078.

(31) Charlebois, P. M.; Corkum, L. D.; Jude, D. J.; Knight, C. The round goby (*Neogobius melanostomus*) invasion: current research and future needs. *J. Great Lakes Res.* **2001**, *27*, 263–266.

(32) Johnson, T. B.; Bunnell, D. B.; Knight, C. T. A potential new energy pathway in central Lake Erie: the round goby connection. *J. Great Lakes Res.* **2006**, *31* (Suppl. 2), 238–251.

(33) Painter, S.; Marvin, C.; Rosa, F.; Reynoldson, T. B.; Charlton, M. N.; Fox, M.; Thiessen, P. A. L.; Estenik, J. F. Sediment contamination in Lake Erie: A 25-year retrospective analysis. *J. Great Lakes Res.* **2001**, *27*, 434–448.

(34) Shimoda, Y.; Azim, M. E.; Perhar, G.; Ramin, M.; Kenney, M.; Sadraddini, S.; Arhonditsis, G. B. Our current understanding of lake ecosystem response to climate change: what have we learnt from the deep lakes?. *J. Great Lakes Res.* **2010**.

(35) Morrison, H. A.; Whittle, D. M.; Haffner, G. D. A comparison of the transport and fate of polychlorinated biphenyl congeners in three Great Lakes food webs. *Environ. Toxicol. Chem.* **2002**, *21*, 683–692.

(36) Stow, C. A.; Carpenter, S. R.; Eby, L. A.; Amrhein, J. F.; Hesselberg, R. J. Evidence that PCBs are approaching stable concentrations in Lake Michigan fishes. *Ecol. Appl.* **1995**, *5*, 248–260.

(37) Stow, C. A.; Jackson, L. J.; Carpenter, S. R. A mixed order model to assess contaminant declines. *Environ. Monit. Assess.* **1999**, *55*, 435–444.

(38) Ellison, A. M. An introduction to Bayesian Inference for ecological research and environmental decision-making. *Ecol. Appl.* **1996**, *6*, 1036–1046.

DETECTION OF THE SPATIOTEMPORAL TRENDS OF MERCURY IN LAKE ERIE FISH COMMUNITIES: A BAYESIAN APPROACH

(Electronic Supplementary Material)

**M. Ekram Azim¹, Ananthavalli Kumarappah¹, Satyendra P. Bhavsar^{2,3}, Sean M. Backus⁴, and
George Arhonditsis^{1,3*}**

¹Ecological Modeling Laboratory
Department of Physical and Environmental Sciences
University of Toronto, Toronto, Ontario, M1C 1A4, Canada

²Environmental Monitoring and Reporting Branch,
Ontario Ministry of the Environment,
Toronto, Ontario, M9P 3V6, Canada

³Centre for Environment
University of Toronto, Toronto, Ontario M5S 3E8

⁴Water Quality Monitoring & Surveillance Division, Water Science and Technology Directorate,
Environment Canada, Burlington, Ontario L7R 4A6

*Corresponding author

E-mail: georgea@utsc.utoronto.ca; Tel: +1 416-208-4858; Fax: +1 416-287-7279

1) SAMPLE EXTRACTION AND ANALYSIS.

The OMOE samples were analyzed for mercury concentrations using the OMOE method HGBIO-E3057 [1]. Briefly, mercury in a skinless, boneless fillet of the dorsal muscle of each fish was oxidized to its divalent ion form by an acid digestion as follows. Frozen fish tissue samples were thawed and then 0.2-0.4 g of tissue were transferred into Folin-Wu digestion tubes using a spatula. Five ml of a 4:1 sulphuric:nitric acid mixture were added to each tube, which were placed in aluminium blocks on hot plates and digested overnight at a temperature of 215-235°C. The samples were cooled and brought up to 25 ml with pure water. A blank and four mercury calibration standards, made from a stock solution traceable to the National Institute of Standards and Technology (NIST), were taken through the same digestion procedure. The calibration was checked with a NIST traceable solution (NIST991304). The correlation coefficient of the regression slope was between 0.99-1.00. The calibration standards were re-analyzed at the end of the run. There was no more than a 10% change in the sensitivity throughout the run. The digestion efficiency was checked against two in-house reference materials. One sample and one in-house reference material were analyzed in duplicates. Recoveries were monitored by spiking both the sample and reference material. After cooling, the sample, calibration, and reference solutions were placed in an automated sampler. The solutions were transferred to a cold vapour flameless atomic absorption spectroscopy (CV-FAAS) system by a peristaltic pump. The mercury was then reduced by a stannous chloride solution (stannous chloride, sodium chloride, hydroxylamine sulphate and concentrated hydrochloric acid) to its elemental form. An air stream carries the mercury vapour through a gas-liquid separator and an impinger containing sulphuric acid into a flow-through elemental mercury detector (Milton Roy) with a light source, set at 253.7 nm wavelength. The detector was heated to remove water. The amount of light absorption was proportional to the concentration of mercury. Signals were processed using a computer with analog-digital converter and appropriate software (Labtronics DP1000) to allow for calculation and reporting.

EC samples were analyzed at the National Laboratory for Environmental Testing using the NLET method 2801 [2]. Mercury concentration in biota is determined by employing the cold vapour absorption spectrometry procedure (VVAAS). First, one gram of wet biota is placed in a 120 mL TFM digestion vessel. Nitric acid and hydrogen peroxide (8:1 mL) are added and mixed with the sample. The vessel is assembled, sealed and fitted into a microwave rotor which is placed in a high pressure microwave oven. The sample is digested and the temperature is maintained at 200 °C for 15 minutes. Mercury (II) in the digest is reduced to elemental mercury in an automated continuous flow system by the action of stannous chloride. The mercury is sparged from the solution with a stream of purified air and passed through an absorption cell, which is situated in the pathway of a mercury lamp. The absorption is measured at 253.7 nm.

References

- [1] *The determination of mercury in biomaterials by cold vapour-flameless atomic absorption spectroscopy (CV-FAAS)*; Ontario Ministry of the Environment: Toronto, Ontario, Canada, 2006.
- [2] Environment Canada *NLET Schedule of Services. The National Laboratory for Environmental Testing*; Water Science and Technology Directorate, Environment Canada: Burlington, Ontario, Canada, 2008.

2) SENSIVITY ANALYSIS OF THE EXPONENTIAL DECAY MODEL

The robustness of the results derived from the exponential decay model when different prior distributions are assigned to the initial mercury concentrations was further examined with the walleye *SBF* data (Table 1-ESM). Priors 1, 4 and 5 resulted in relatively similar posterior Hg_0 estimates (around $0.3 \mu\text{g THg/g}$ wet weight), while Priors 2 and 3 predicted substantially higher values ($0.748 \pm 1.586 \mu\text{g THg/g}$ and $0.587 \pm 0.218 \mu\text{g THg/g}$). We also highlight that the use of flat Hg_0 prior (Prior 2) led to a poorly determined posterior estimate. Interestingly, despite the use of similar flat prior distributions for the decay rates (k), the corresponding posteriors were higher with the Priors 2 ($-0.070 \pm 0.050 \text{ yr}^{-1}$) and 3 ($-0.077 \pm 0.028 \text{ yr}^{-1}$), followed by the Prior 1 ($-0.049 \pm 0.025 \text{ yr}^{-1}$) and then the Priors 5 ($-0.037 \pm 0.029 \text{ yr}^{-1}$) and 4 ($-0.029 \pm 0.035 \text{ yr}^{-1}$). Thus, whilst the measurement error σ_e as well as the conditional standard deviations of the δ_t terms (ω) associated with the different specifications were very similar, the posterior parameter values appear to be somewhat sensitive to the assumptions made regarding the Hg_0 prior values. We also note that the Hg_0 and k values suggest positive covariance, although the explicit consideration of such term (σ_{kHg_0}) did not unequivocally resolve the strength of their relationship (0.019 ± 8.077). Importantly, the comparison of the δ_t terms derived from the five prior assumptions consistently reveals an increasingly positive structural error after the mid-90s, indicative of the structural deficiency of the single exponential model to describe the recently increasing Hg trends (Fig. 2-ESM). Generally, our sensitivity analysis suggests that the conclusions drawn upon the general THg temporal patterns are robust, although that actual parameter estimates can differ depending on the prior assumptions made about the relative plausibility of their values.

3) HIERARCHICAL SPATIAL MODEL

The outcomes of the hierarchical spatial model developed using the walleye *SBF* data for the four locations in Lake Erie (Western Basin, Central Basin, Long Point Bay and Eastern Basin) are shown in Fig. 7-ESM. The parameter estimates for k_1 and k_2 derived from the double exponential model (-0.133 ± 0.018 and 0.056 ± 0.008 yr^{-1}) with all the data pooled were quite close to the hyperparameter estimates of the hierarchical model (-0.162 ± 0.097 and 0.044 ± 0.109 yr^{-1}). The rates of mercury decline in walleye were predicted to be higher in the Central Basin ($k_1=-0.184\pm 0.024$ yr^{-1} ; Fig. 7b-ESM) and Eastern Basin ($k_1=-0.177\pm 0.032$ yr^{-1} ; Fig. 7d-ESM) followed by Western Basin ($k_1=-0.141\pm 0.017$ yr^{-1} ; Fig. 7a-ESM) and the Long Point Bay ($k_1=-0.078\pm 0.020$ yr^{-1} ; Fig. 7c-ESM). Yet, the latter k_1 estimate should be interpreted with caution, as we completely lack data from Long Point Bay before 1989. By contrast, the walleye samples collected from the Eastern Basin exhibited relatively higher rate of increase in *THg* concentrations ($k_2=0.056\pm 0.006$ yr^{-1} ; Fig. 7d-ESM) than those collected from other locations ($k_2=0.037$ - 0.044 yr^{-1}). The decline in *THg* concentrations continued until 1992 in the Western Basin, and until 1986 in both Central and Eastern Basins after which they started to increase again (Fig. 7a to c-ESM).

4) TABLES

Table 1-ESM: Sensitivity analysis of the *SBF* walleye mercury exponential decay model with 1st order random walk using different prior specifications. *Prior 1* denotes an informative normal Hg_0 prior derived from the mercury concentrations measured in 1976; *Prior 2* denotes non-informative prior parameter distributions; *Prior 3* and *Prior 4* denote normally and log-normally distributed Hg_0 priors, parameterized such that 99% of the respective values were lying within the minimum and maximum mercury concentrations measured in 1976; and *Prior 5* denotes multivariate normal priors that account for the covariance between the parameters Hg_0 and k .

| | Prior 1 | | Prior 2 | | Prior 3 | | Prior 4 | | Prior 5 | |
|----------------------|---------|-------|---------|-------|---------|-------|---------|-------|---------|-------|
| | Mean | SD |
| Hg_0 | 0.375 | 0.136 | 0.748 | 1.586 | 0.587 | 0.218 | 0.297 | 0.182 | 0.326 | 0.196 |
| k | -0.049 | 0.025 | -0.070 | 0.050 | -0.077 | 0.028 | -0.029 | 0.035 | -0.037 | 0.029 |
| ω | 0.252 | 0.041 | 0.263 | 0.049 | 0.264 | 0.043 | 0.250 | 0.041 | 0.249 | 0.041 |
| σ_ε | 0.481 | 0.008 | 0.481 | 0.008 | 0.481 | 0.008 | 0.481 | 0.008 | 0.481 | 0.008 |
| σ_k | | | | | | | | | 0.392 | 0.497 |
| σ_{Hg_0} | | | | | | | | | 0.569 | 0.913 |
| σ_{kHg_0} | | | | | | | | | 0.019 | 8.077 |

5) FIGURES

Figure 1-ESM: Map of Lake Erie with the four sampling sites: 1: Western Basin, 2: Central Basin, 3: Long Point Bay, and 4: Eastern Basin.

Figure 2-ESM: Sensitivity of the first-order random walk terms (δ_t) of the SBF walleye mercury exponential decay model using different prior specifications. *Prior 1* denotes an informative normal Hg_0 prior derived from the mercury concentrations measured in 1976; *Prior 2* denotes non-informative prior parameter distributions; *Prior 3* and *Prior 4* denote normally and log-normally distributed Hg_0 priors, parameterized such that 99% of the respective values were lying within the minimum and maximum mercury concentrations in 1976; and *Prior 5* denotes multivariate normal priors that account for the covariance between the parameters Hg_0 and k .

Figure 3-ESM: Mercury concentrations over time (1970-2007) using the exponential decay model with (a, b) yellow perch skinless-boneless fillet, (c, d) smallmouth bass skinless-boneless fillet and (e, f) white bass skinless-boneless fillet data from Lake Erie. The circles indicate the observed values, while the solid and dashed lines correspond to the median and the 95% credible intervals of the posterior predictive distributions, respectively. The δ annual values correspond to the first-order random walk terms introduced to account for the structural deficiencies of the single exponential model.

Figure 4-ESM: Walleye mercury concentrations over time (1976-2007) using the mixed-order model with (a, b) whole fish, and (c, d) skinless-boneless fillet data for Lake Erie. The circles indicate the observed values, while the solid and dashed lines correspond to the median, and the 95% credible intervals of the posterior predictive distributions, respectively. The δ_t annual values correspond to the first-order random walk terms introduced to account for the structural deficiencies of the single exponential model.

Figure 5-ESM: Mercury concentrations over time (1970-2007) using the mixed-order model with (a, b) yellow perch skinless-boneless fillet, (c, d) smallmouth bass skinless-boneless fillet and (e, f) white bass skinless-boneless fillet data from Lake Erie. The circles indicate the observed values, while the solid and dashed lines correspond to the median and the 95% credible intervals of the posterior predictive distributions, respectively. The δ annual values correspond to the first-order random walk terms introduced to account for the structural deficiencies of the mixed-order model.

Figure 6-ESM: Mercury concentrations over time (1976-2007) using the double exponential model with (a) whole fish walleye, (b) skinless-boneless fillet walleye, (c) skinless-boneless fillet yellow perch, (d) skinless-boneless fillet smallmouth bass, and (e) skinless-boneless fillet white bass for Lake Erie. The circles indicate the observed values, while the solid and dashed lines correspond to the median and the 95% credible intervals of the posterior predictive distributions, respectively.

Figure 7-ESM: Observed (circles) versus predicted median (solid line) mercury concentrations ($\mu\text{g/g}$ wet weight) in walleye SBF data for four regions in Lake Erie (a: Western Basin, b: Central Basin, c: Long Point Bay, and d: Eastern Basin) using the hierarchical double exponential model. Dashed lines correspond to the 95% credible intervals.

**Lake Erie
Lac Érié**

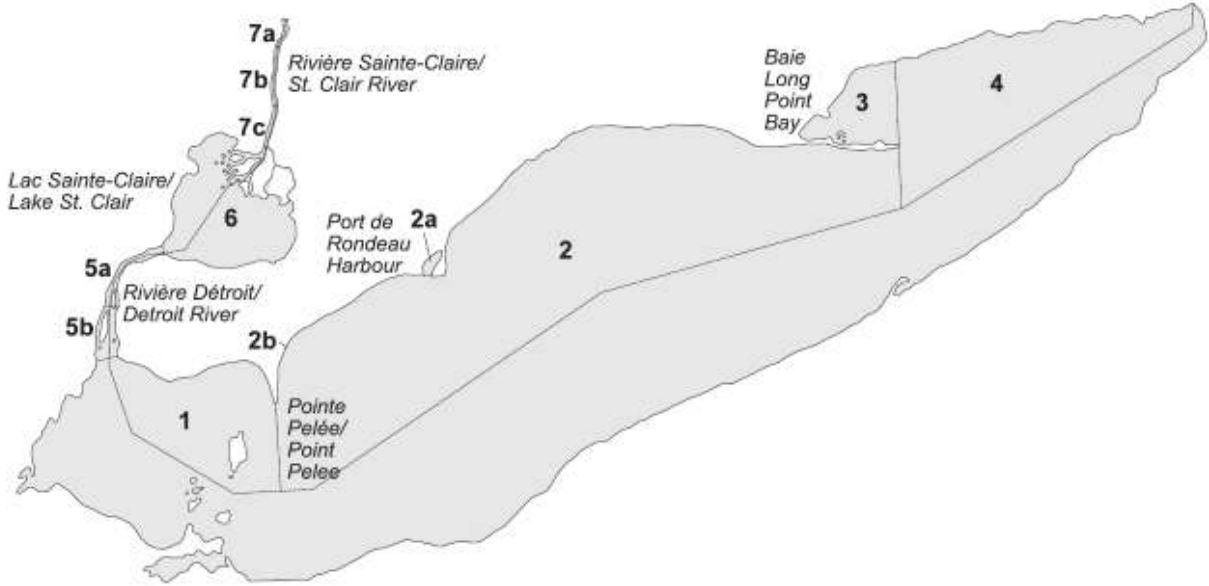


Figure 1-ESM

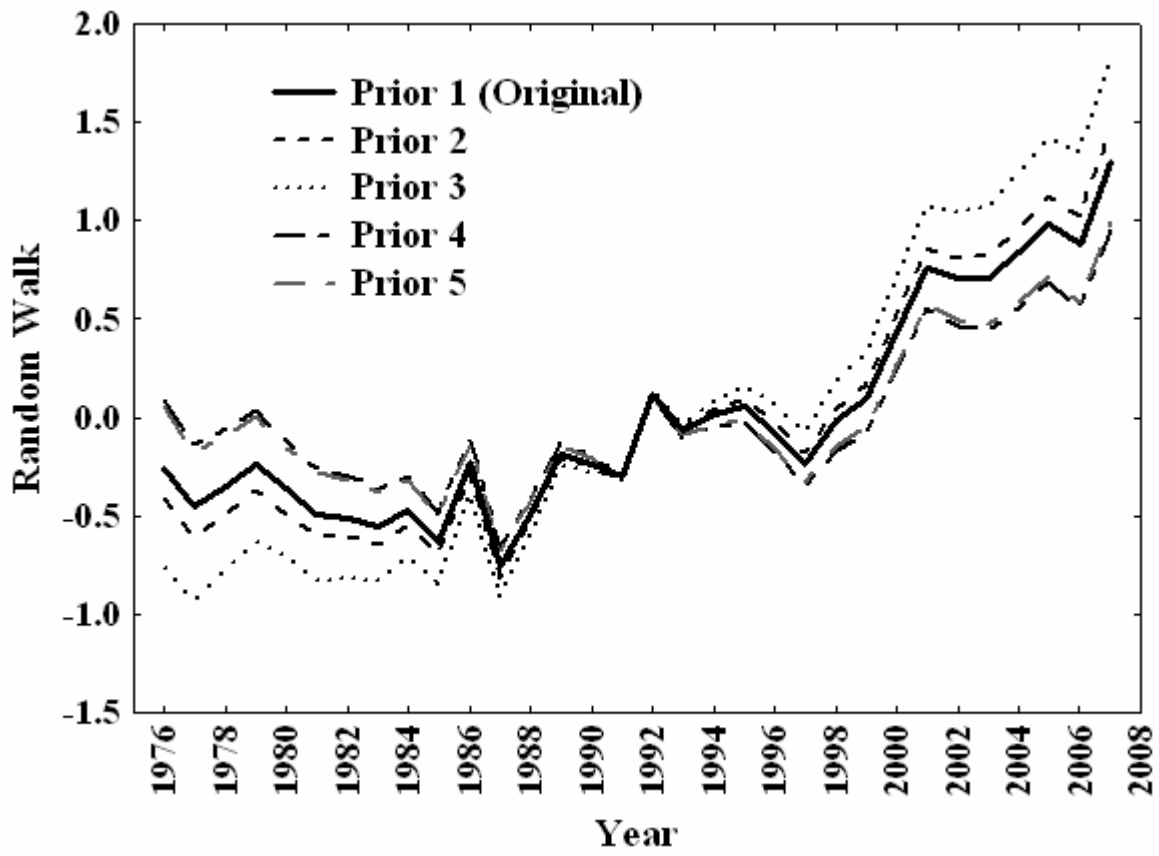


Figure 2-ESM

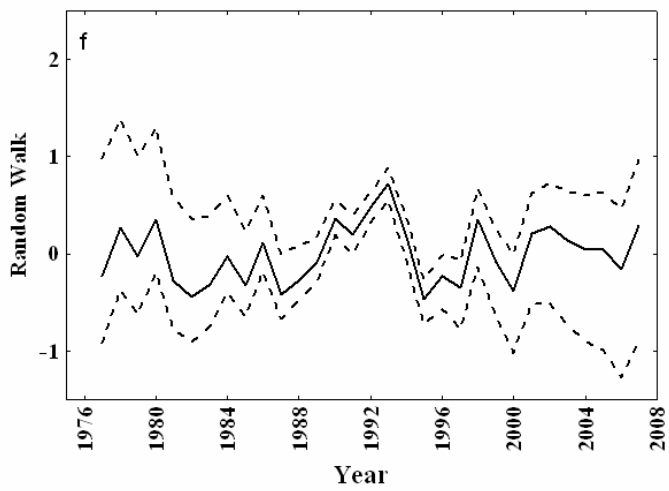
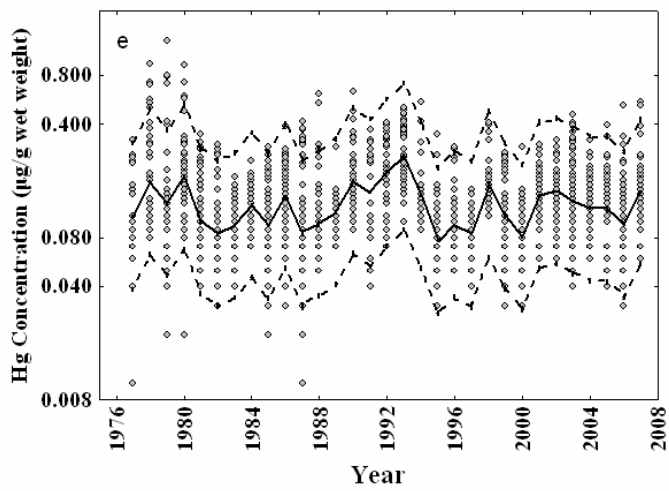
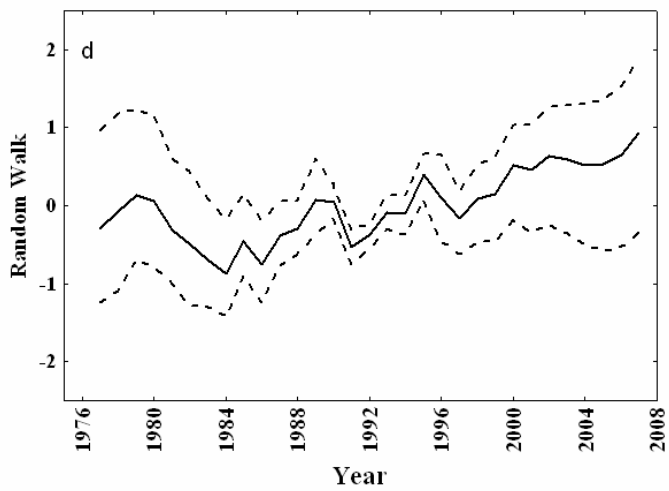
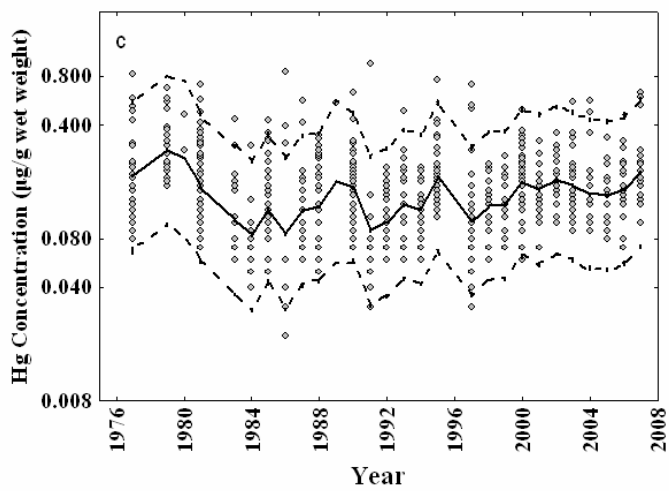
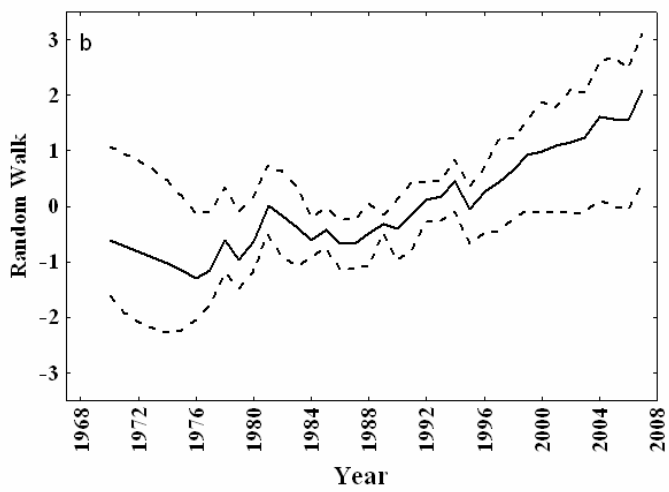
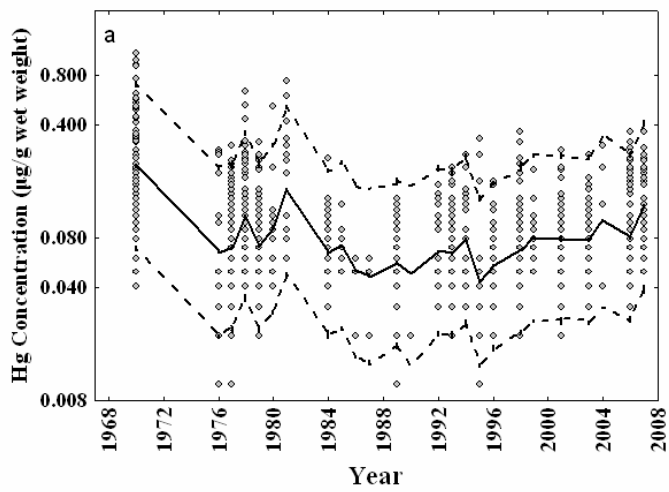


Figure 3-ESM

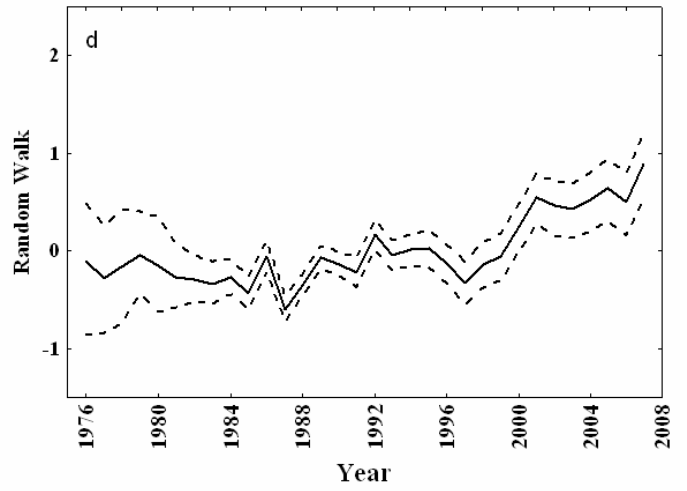
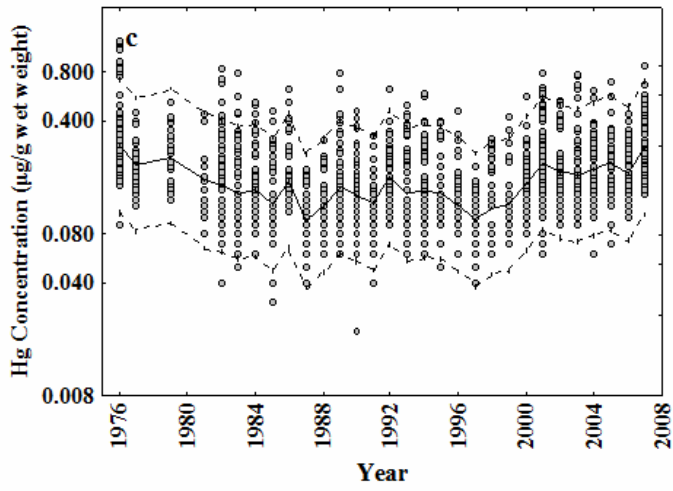
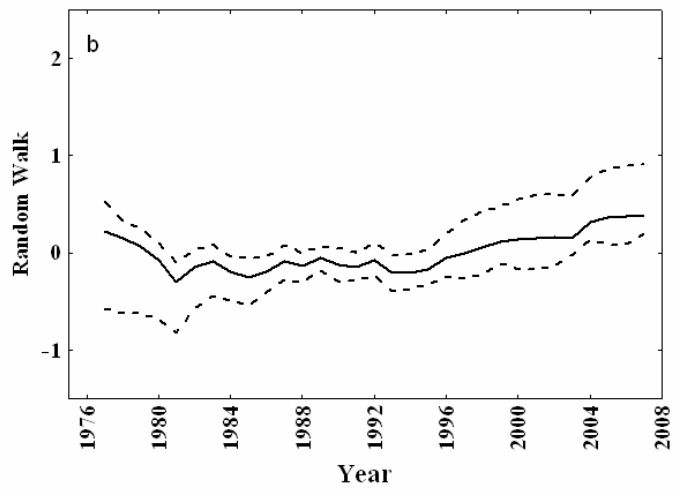
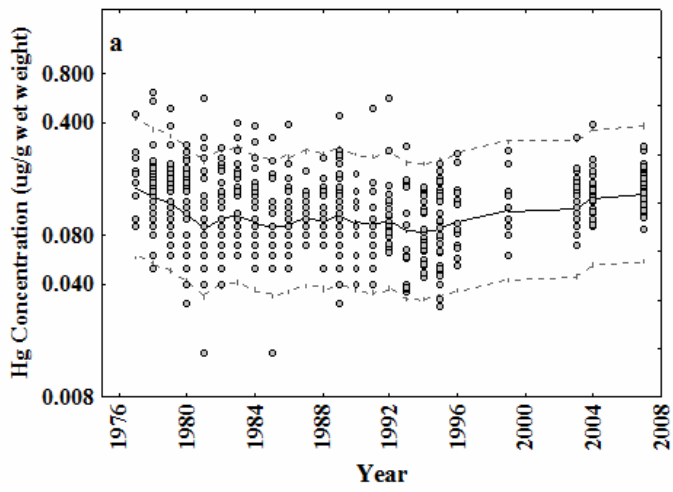


Figure 4-ESM

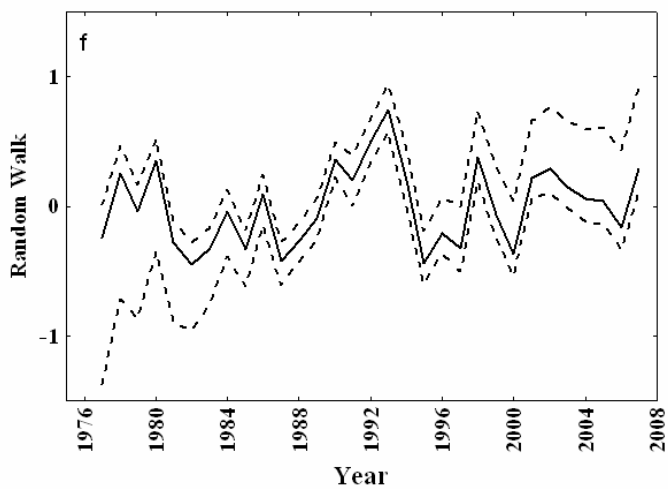
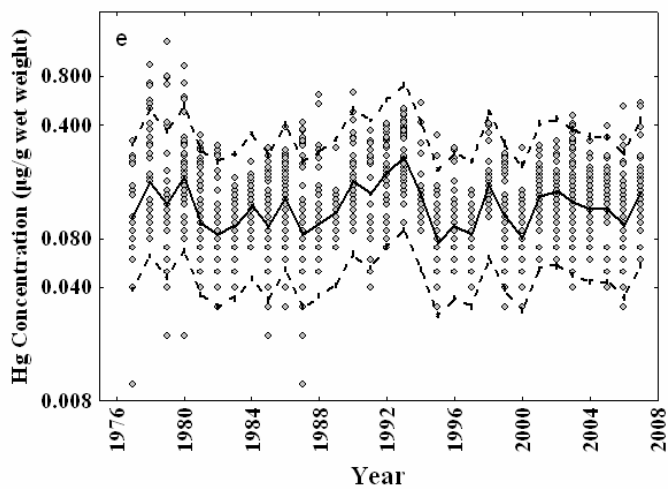
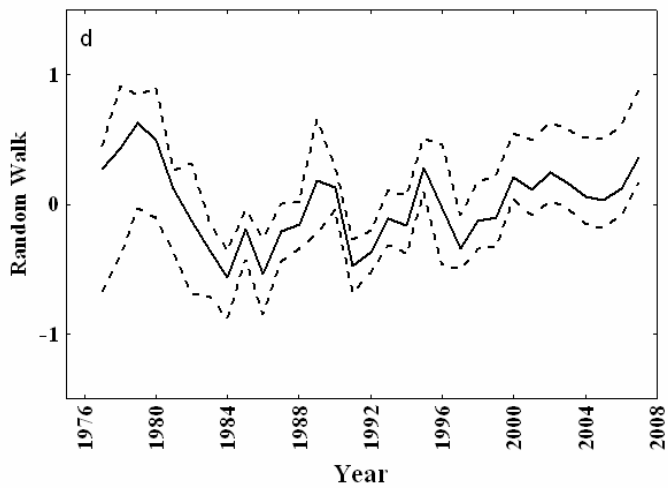
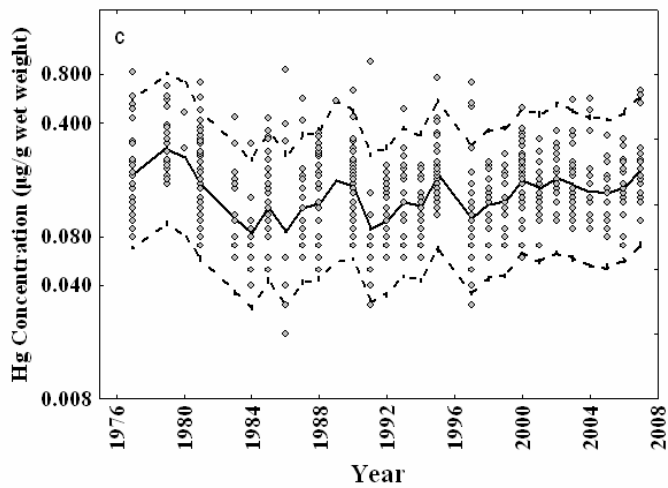
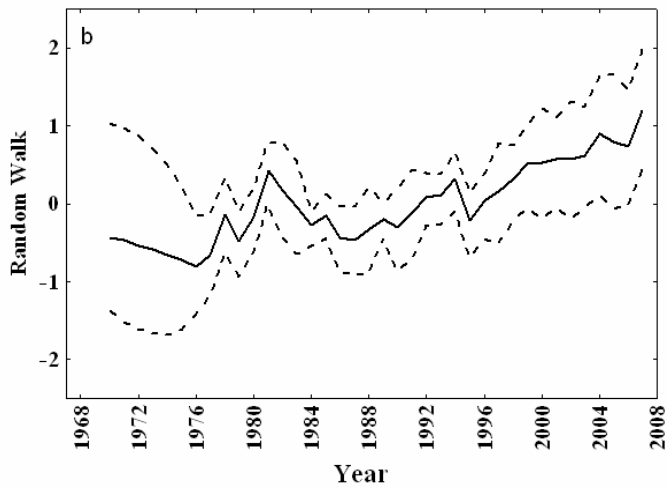
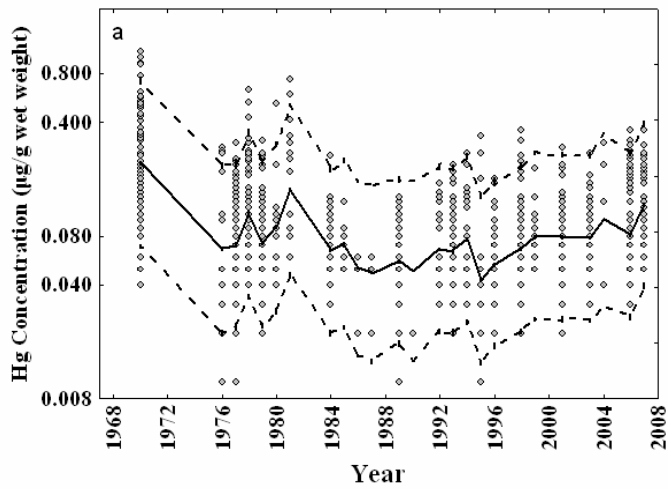


Figure 5-ESM

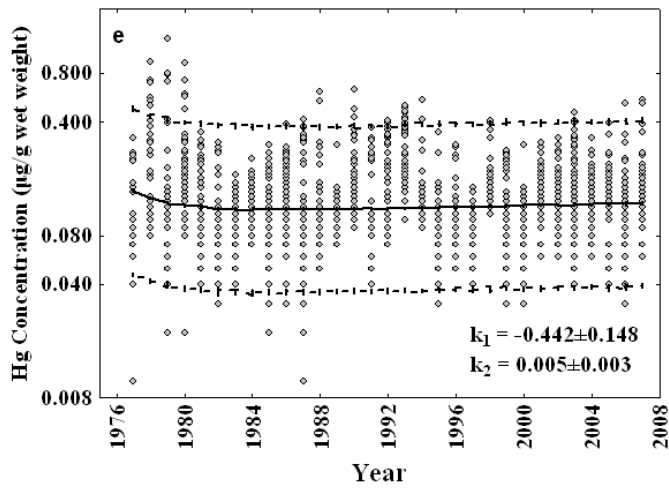
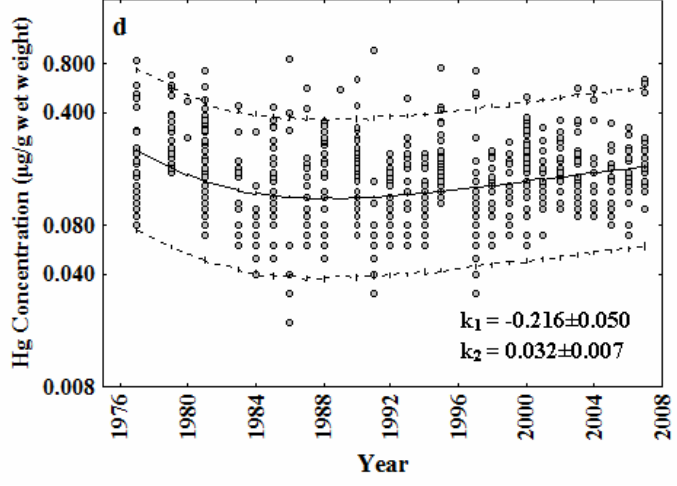
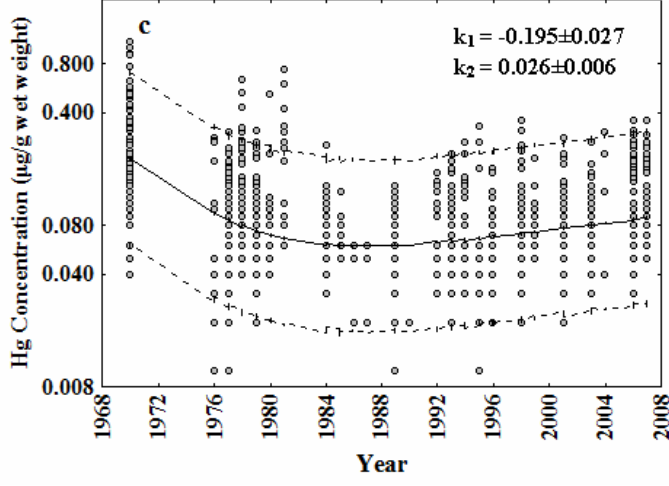
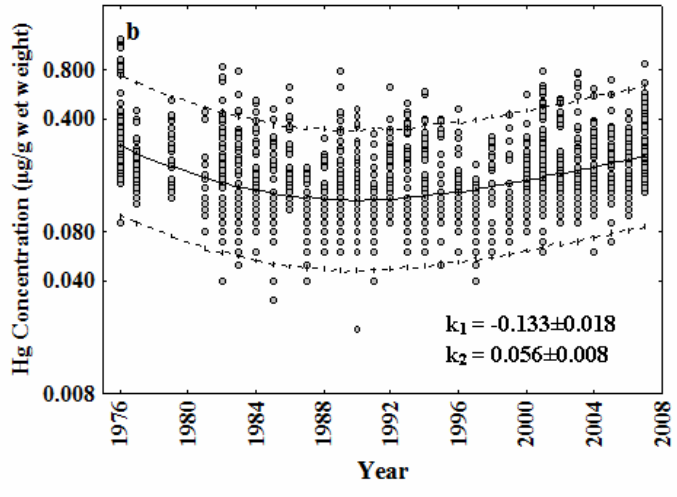
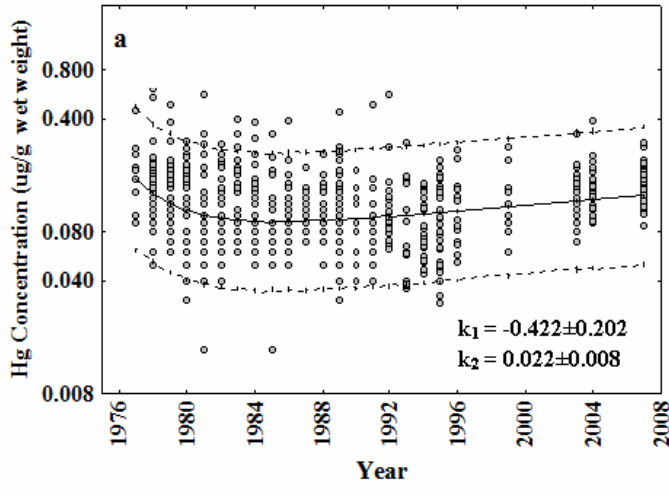


Figure 6-ESM

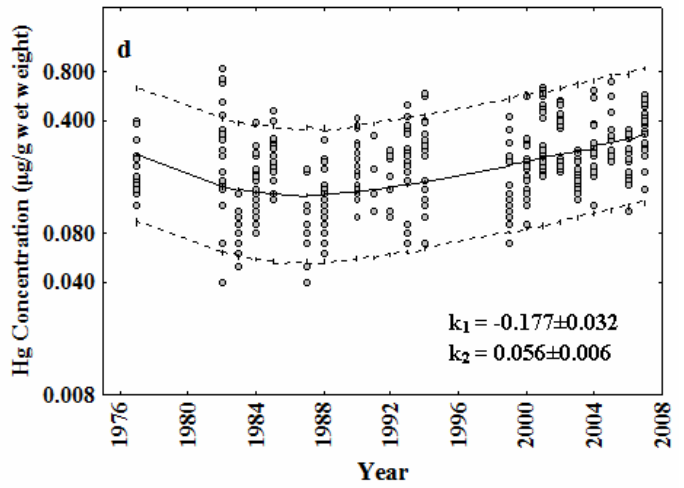
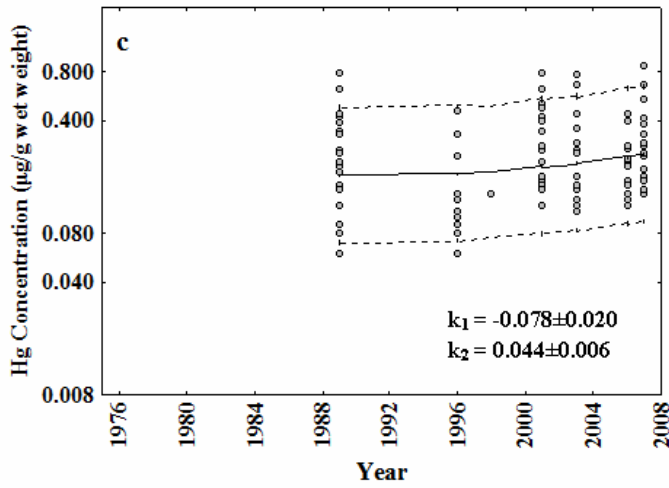
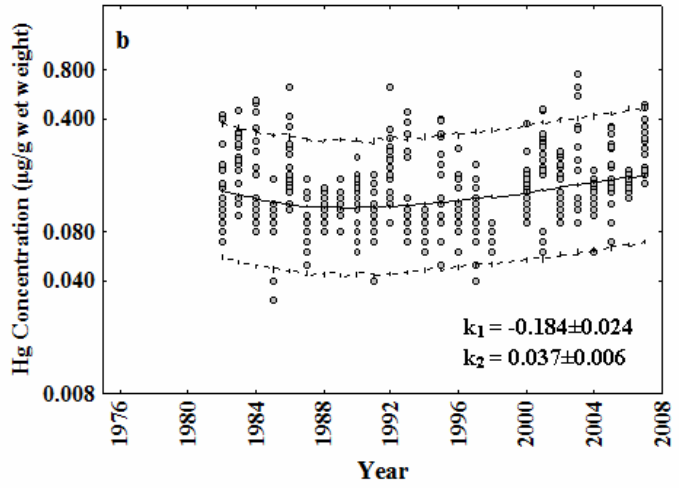
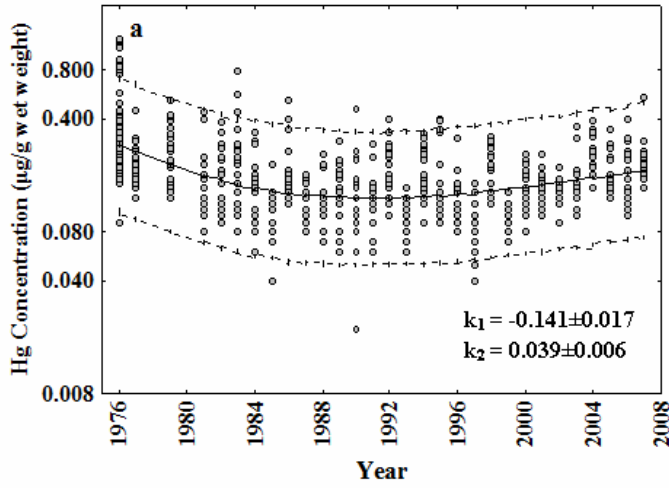


Figure 7-ESM